Electronic Supplementary Material (ESI) for Chemical Science.
This journal is © The Royal Society of Chemistry 2018

Electronic Supplementary Information

for

Probing Surfaces of Atmospherically Relevant Organic Particles by Easy Ambient Sonic-Spray Ionization Mass Spectrometry (EASI-MS)

L. M. Wingen and B. J. Finlayson-Pitts

Department of Chemistry

University of California Irvine

Irvine, CA 92697-2025

1. Polydisperse particle size distributions of glutaric acid particles and malonic acid-coated glutaric acid particles.

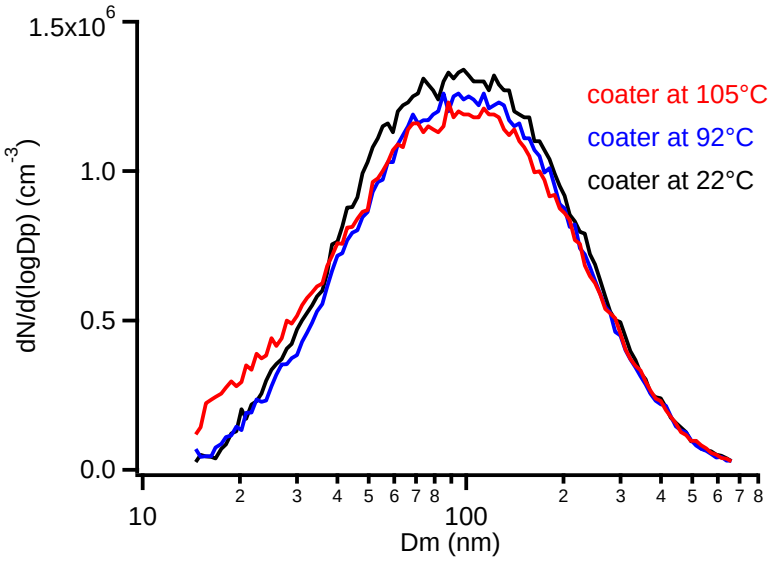

Figure S1. Polydisperse size distributions of glutaric acid particles with coatings generated from malonic acid in the reservoir heated to 22°C, 92°C, and 105°C, respectively. Total number concentrations are 1.1×10^6 cm^{-3} in all cases.

2. Typical mass spectra collected in droplet mode EASI-MS.

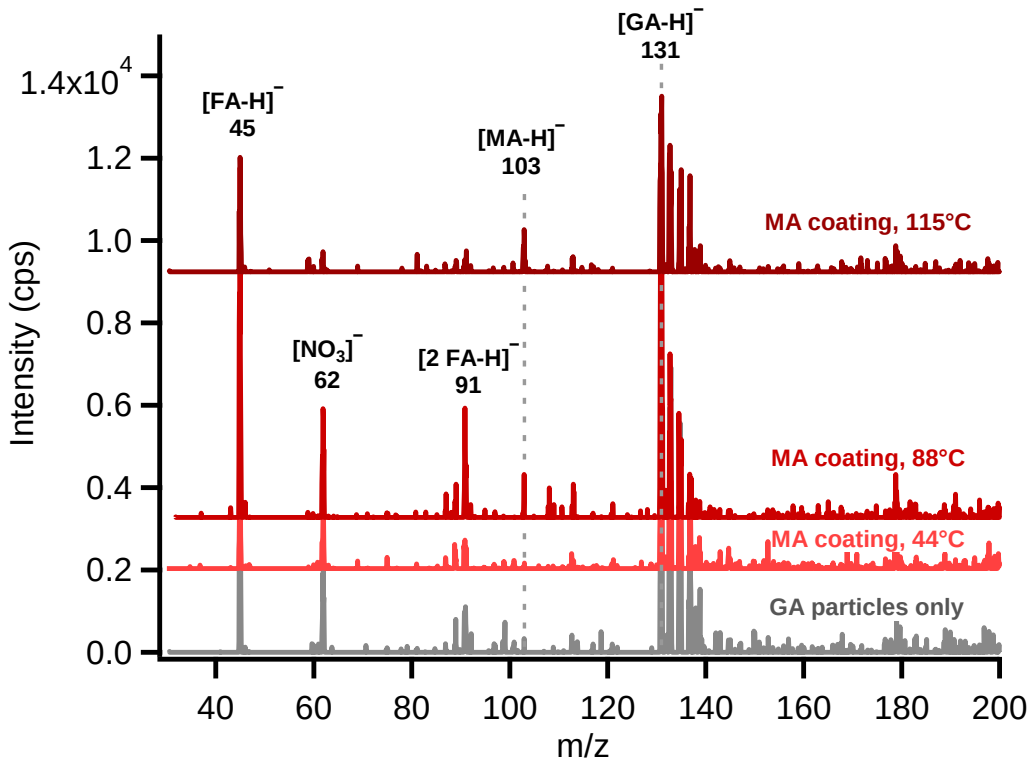

Figure S2. EASI-MS spectra collected in the droplet mode of MA-coated polydisperse GA particles as a function of coating reservoir temperature. The GA peak (*m/z* 131, $[GA\text{-}H]^-$) is relatively constant with increasing MA temperature, while the MA peak (*m/z* 103, $[MA\text{-}H]^-$) increases. Spectra are averaged over 1 – 2 minutes and have had solvent subtracted (also averaged over 1 – 2 minutes). Particle flow was sent through a charcoal denuder to remove vapor phase MA. FA = formic acid present in the solvent. NO_3^- (*m/z* 62) is a common fragment in ambient negative ion mode spectra.[1]

The cluster of peaks at *m/z* 133, 135, 137, and 139 is from $CuCl_2$ impurities traced to chloride in the formic acid and copper in the laboratory air, possibly from the building air handling lines,[2] which are difficult to remove with solvent subtractions. The relative peak intensities from the isotopes $^{63}Cu^{35}Cl_2$ (*m/z* 133), $^{65}Cu^{35}Cl_2$ and $^{63}Cu^{35}Cl^{37}Cl$ (*m/z* 135), $^{63}Cu^{37}Cl_2$ and $^{65}Cu^{35}Cl^{37}Cl$ (*m/z* 137), and $^{65}Cu^{37}Cl_2$ (*m/z* 139) confirm the assignment.

3. Suppression of carboxylic acids in solution.

The MA/GA ratios from the bulk analysis of both analytes in the nebulizer solution at the highest coating reservoir temperature were higher than those from the droplet mode, by 35-70%, as shown in Fig. 6b (main text). This is due to the suppression of the GA signal by the stronger acid, MA, an effect that has been observed in negative ion mode ESI-MS of carboxylic acid solutions containing more than one acid.[3] Ion suppression was investigated in separate experiments in which equimolar solutions of MA and GA were analyzed with EASI-MS. The peak height of GA was smaller than that of MA by a factor of 1.8 – 1.9 in solutions of equimolar MA and GA at concentrations ranging from 1.7 – 17 μM. Figure S3 shows a droplet mode EASI-MS spectrum of equimolar 17 μM MA and GA in which the GA peak (*m/z* 131, $[GA\text{-}H]^-$) is a factor of 1.9 lower than would be expected if the two acids had similar ionization efficiencies (see Fig. S4). Similar levels of suppression were observed for 8.5 μM and 1.7 μM equimolar solutions of MA and GA. However, solutions in which GA was in excess of MA by ~8:1 (17 μM GA, 2 μM MA) did not exhibit suppression of GA.

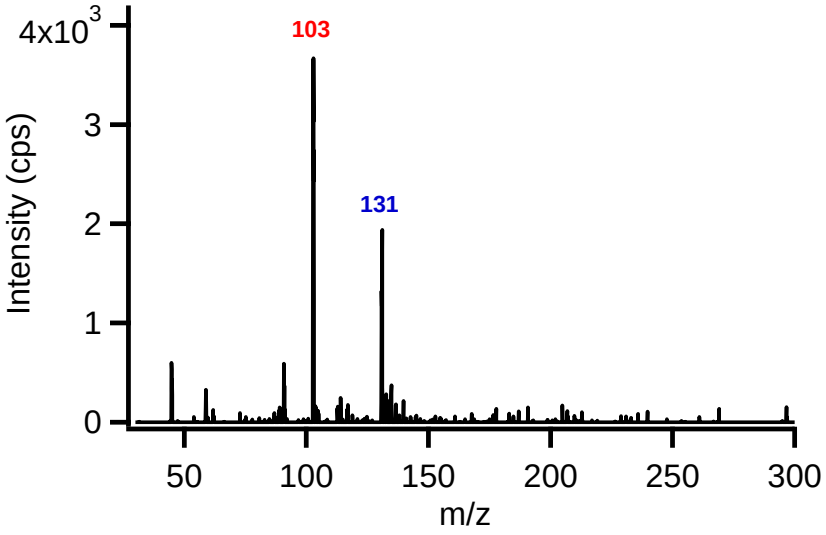

Figure S3. EASI-MS spectra collected in the droplet mode of an equimolar solution of 17 μM MA and GA. GA is suppressed by a factor of 1.9 in solution.

In comparison, Figure S4 shows two spectra obtained separately of 1.05 mM malonic acid and 0.96 mM glutaric acid by nebulizing each solution in droplet mode. The two diacids were detected with approximately equal intensities in the mass spectrometer, indicating they have similar ionization efficiencies. Peaks were also observed for dimers at the higher concentrations used in Fig. S4, *m/z* 207 $(2MA\text{-}H)^-$ and *m/z* 263 $(2GA\text{-}H)^-$.

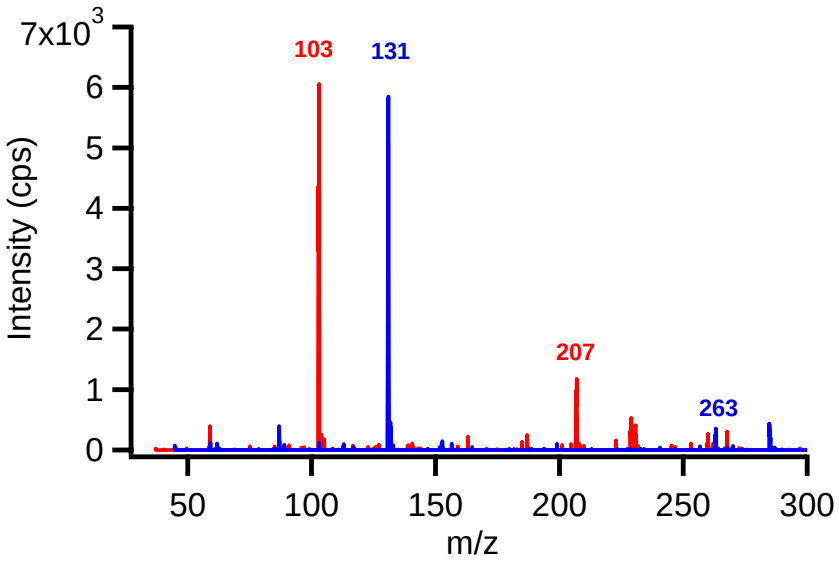

Figure S4. Droplet mode EASI-MS spectra collected for separate solutions of 1.05 mM MA (red) and 0.96 mM GA (blue). Each diacid, MA (*m/z* 103) and GA (*m/z* 131), has approximately the same peak height and thus similar ionization efficiencies.

Additional experiments were carried out with separate flows of dry, polydisperse MA and GA particles intersecting the nebulizer in droplet mode. Introduction of GA particles alone followed by GA particles and MA particles from separate streams did not result in ion suppression and similar intensities were observed for GA particles as MA particles were introduced. Figure S5 confirms that signal suppression is observed only for solutions inside the EASI nebulizer and does not affect solid particle analysis.

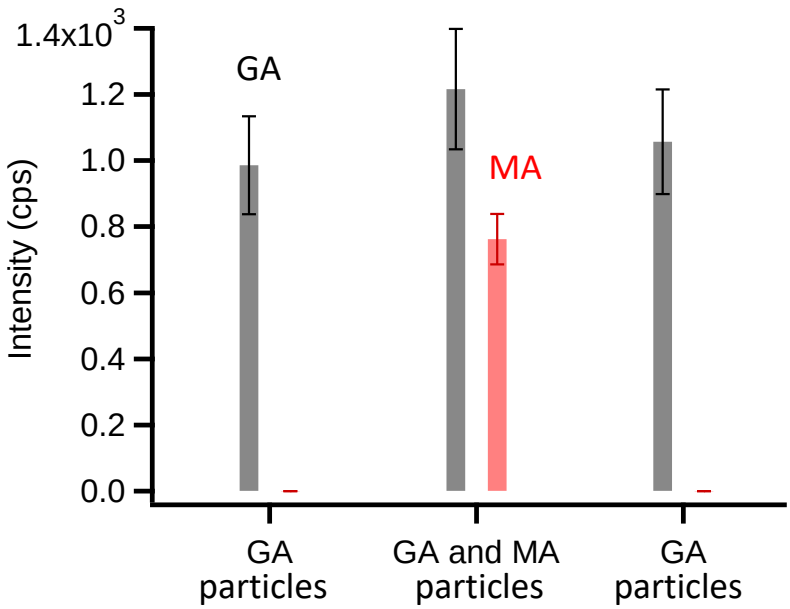

Figure S5. Droplet mode EASI-MS peak heights of GA (grey) and MA (red) in which a GA particle stream was analyzed (GA particles), then an MA particle stream was introduced (GA and MA particles), and finally the MA particle stream was removed (GA particles). Peak intensities show that the introduction of MA particles separately does not cause suppression of the GA particle signal. Error bars represent typical 2s uncertainties.

4. Measurement and evaporation of coated monodisperse particles.

Measurements of monodisperse glutaric acid (GA) particles by SMPS exhibited unexpectedly low particle diameters than selected using DMA-1. For example, in Figure S6, size selection of 250 nm GA particles was performed with DMA-1 and measured with SMPS, resulting in a measured mode diameter of 217 nm (black trace). This diameter is 13% lower than expected and is not within the uncertainty established through diameter calibrations with CMLs (see main text). Measured diameters of GA particles were consistently smaller than those selected by setting the appropriate voltage on DMA-1, with larger deviations for smaller particles. For example, size-selected 100 nm GA particles were observed to have a mode of 62 nm (see main text and section 6 below). However, SMPS-measured diameters of size-selected

succinic acid (SA), adipic acid (AA) and pimelic acid (PA) particles, shown in Figure S6, were within the uncertainty of the CML calibrations performed on DMA-1 and the SMPS. This is consistent with evaporative loss for GA since succinic, adipic, and pimelic acids each have lower vapor pressures than glutaric acid.[4,5]

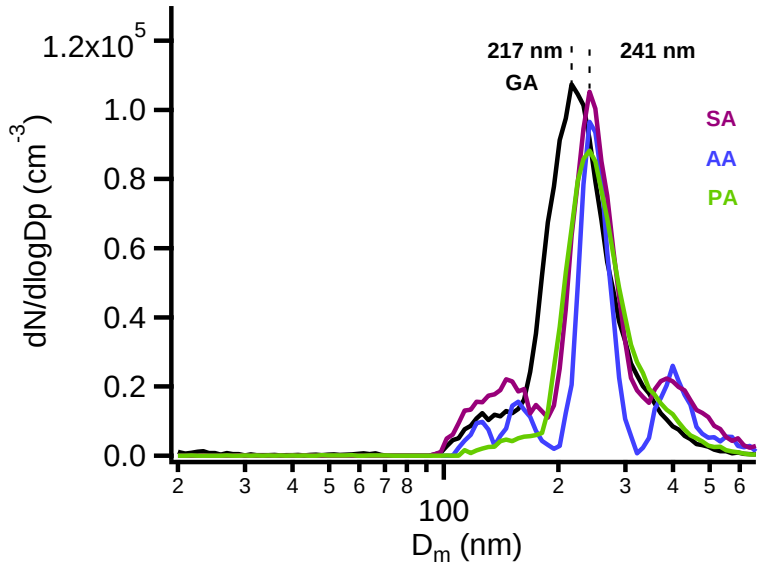

Figure S6. SMPS-measured size distributions of size-selected 250 nm uncoated succinic acid (purple), adipic acid (blue), and pimelic acid (green) particles. The mode of each is observed at 241 nm and is within the uncertainty of SMPS-2 measured with CMLs.[6] Also shown is an SMPS-measured size distribution of size-selected 250 nm uncoated glutaric acid (black), with a measured mode of 217 nm, which is outside the uncertainty of SMPS-2.

Selected measurements were carried out with an aerodynamic aerosol classifier (AAC, Cambustion, Ltd., Cambridge, UK).[7-9] The AAC measures aerodynamic diameter, d_a, based on particle trajectory under centrifugal forces toward an outer cylinder as sheath air carries them along a rotating inner cylinder. The aerodynamic diameter, d_a, is related to the mobility diameter, d_m, via Eqn. (1), assuming the particles are spherical:[10]

$$d_a = d_m \left[\frac{C_c(d_m)}{C_c(d_a)}\right]^{1/2} \left[\frac{\rho_{eff}}{\rho_0}\right]^{1/2} \quad (1)$$

where $C_c(d_m)$ and $C_c(d_a)$ are the Cunningham slip correction factors for the mobility diameter and corresponding aerodynamic diameter, ρ_{eff} is the effective density of the particle material, and ρ_0 is unit density, 1 g cm^{-3}. The Cunningham slip correction factor is a function of diameter, d, and becomes significant below 1 μm.[10] Values of C_c in the range 100 nm < d < 1000 nm are given by Eqn. (2):

$$C_c = 1 + \frac{2.52\lambda}{d} \quad (2)$$

where λ is the mean free path of air. Since C_c must be determined for both diameters, the calculation of one diameter without knowledge of the other is iterative.

The AAC was used with the CPC (TSI, model 3776) to measure size distributions of glutaric acid particles that were size selected with DMA-1. Particles selected to have an electrical mobility diameter of 250 nm in DMA-1 were measured to have an aerodynamic diameter of 298 nm, corresponding to an electrical mobility diameter of 239 nm (Fig. S7, blue trace), which is only 4% lower than the selected diameter and indicates that less evaporation occurred in the AAC+CPC measurement. The residence time in the AAC at sheath air flows of 2.0 – 2.4 L min^{-1} is 2.9 – 3.5 seconds, while in SMPS at its sheath flow rate of 3 L min^{-1} is 7.5 seconds. AAC has a shorter residence time by a factor of ≥2, consistent with the observation of less evaporation.

Evaporation of diacids has been observed in other studies as well.[11-15] Particles size-selected in DMA-1 to have a 100 nm diameter were not detected with the AAC+CPC, likely due to severe evaporation combined with particle loss in the AAC, which becomes significant below 100 nm.

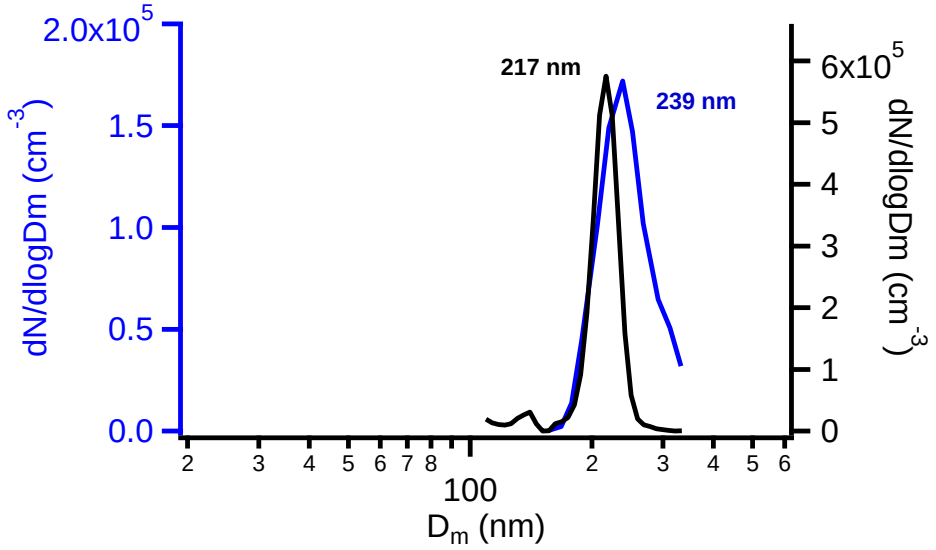

Figure S7. Particle size distributions measured for uncoated glutaric acid particles. Black: 312 nm d_a, corresponding to 250 nm d_m using Eqn. (1), selected with the AAC and measured with SMPS-2. This gave a measured electrical mobility diameter of 217 nm. Blue: 250 nm d_m selected with DMA-1 and measured with the AAC+CPC resulted in a d_a of 298 nm, with a corresponding d_m of 239 nm.

The AAC was also used alone to size-select particles. In this case size distributions were measured with SMPS. Particles were selected with the AAC to have an electrical mobility of 250 nm, by selecting an aerodynamic diameter of 312 nm on the AAC, and were then measured with SMPS. This resulted in GA mode diameters with an electrical mobility diameter of 209 – 217 nm, consistent with evaporation occurring in the DMA and a slightly longer sampling line used to connect the two instruments for these separate experiments.

During experiments in which GA particles were coated with malonic acid, the diameter of the uncoated GA was typically 217 nm or 225 nm. These two diameters are one bin apart in the SMPS in this diameter region, and since SMPS reports midpoint diameters, these data suggest that the true mode diameter is near the endpoint of one bin, i.e. 220 – 221 nm. An example of the reproducibility of uncoated and coated particle diameters is shown in Figure S8, in which particle size distributions were collected while heating the MA to coat monodisperse GA particles and also while cooling MA to decrease the coating and return to bare GA particles.

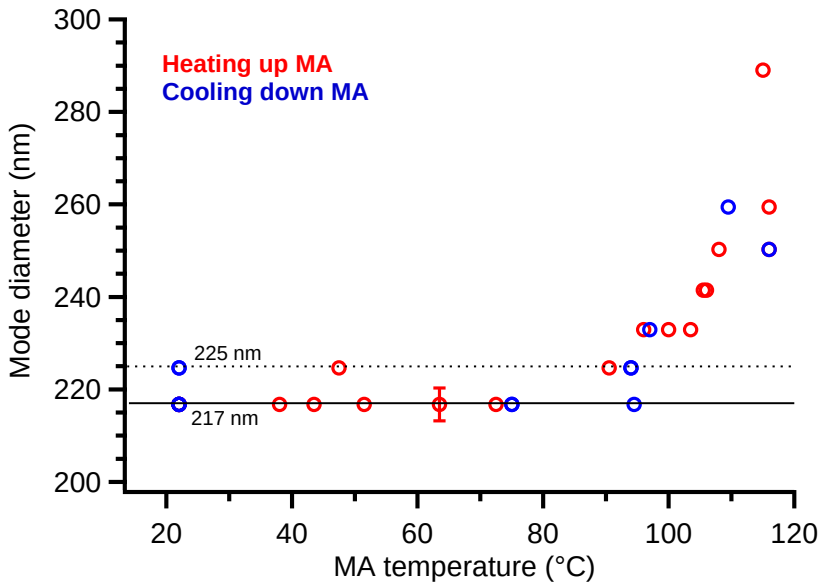

Figure S8. Mobility mode diameter as a function of MA reservoir temperature used to coat monodisperse 250 nm GA particles size-selected with DMA-1 and measured by SMPS. Red circles indicate that MA temperature was being increased to generate a thicker coating of MA on the GA particles. Blue circles indicate MA temperature decreasing. The error bar represents the 1s uncertainty based on replicate measurements of uncoated particles. The uncertainty in the temperature is approximately the width of the markers.

A coating experiment was also carried out in which the size distributions of monodisperse GA particles were measured with the AAC+CPC as a function of MA coating thickness, as described in the main text. Particles were selected by DMA-1 to have an electrical

mobility diameter of 250 nm before flowing through the coating assembly containing MA. Aerodynamic diameter size distributions were measured by the AAC+CPC and converted to mobility diameters using Eqn. (1) – (2). These mobility diameters are shown in Figure S9 as a function of MA coating reservoir temperature using the density of pure GA (d_{GA} = 1.42 g cm^{-3}) in Eqn. (1) (black points). As discussed in the main text, aerodynamic diameter changes with particle density. Thus, the density of coated GA particles will slightly increase as the MA coating (d_{MA} = 1.6 g cm^{-3}) becomes thicker. Based on the volume of 239 nm diameter GA particles coated with a 27 nm-thick shell of MA (from SMPS), the volumes of MA and GA in the particles are approximately 1:1. Using this ratio to calculate a volume-weighted density for the thickest coated particles gives a density of 1.5 g cm^{-3}. Similar calculations were carried out at lower temperatures with thinner detected coatings. Densities were chosen iteratively to match the coating thicknesses at each temperature with the AAC+CPC. These mobility diameters corrected for density are shown in Fig. S9 (red points). Because the densities of MA and GA are similar, the correction is only ~6%. The maximum coating thickness of 33 – 35 nm measured with the AAC+CPC including density corrections is in good agreement with that measured by SMPS, 27 nm, given that the AAC+CPC measurement exhibits less evaporation of GA particles. If the assumption is made that the particle density reaches the density of MA, the maximum coating thickness is calculated to be 30 nm. Thus, the coating thickness as measured by AAC+CPC is not significantly dependent on particle density for this system.

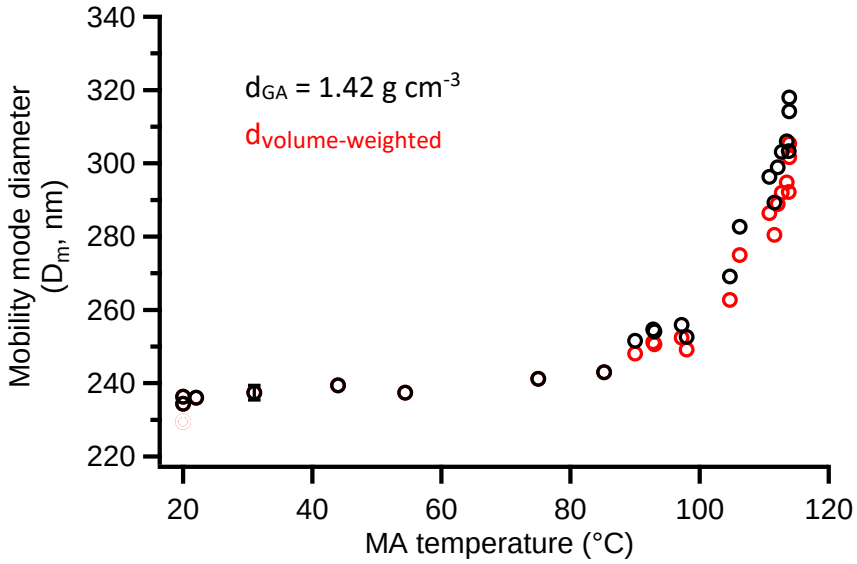

Figure S9. Mobility mode diameters as a function of MA temperature used to coat monodisperse 250 nm GA particles size-selected with DMA-1 and measured with the AAC+CPC. Eqn. (1) and (2) were used to convert the measured aerodynamic diameters to electrical mobility diameters using the density of pure GA (black) or the volume-weighted density of MA-coated GA particles (red). The error bar represents the 1s uncertainty of replicate measurements of uncoated particles by the AAC.

5. Blank experiment with uncoated monodisperse GA particles.

Figure S10 shows data from an experiment in which the coating reservoir was empty to check for particle growth and evaporation during heating of the reservoir. Particles were size selected at 250 nm with DMA-1 and flowed through the empty coating reservoir. As the temperature of the empty coater increased, the orthogonal EASI-MS intensity of the uncoated GA particles did not decrease (Fig. S10a) and the particle diameters remained constant at 217 nm Fig. S10b). These data indicate that particles did not further evaporate, decompose, or aggregate when the heated air stream combined with the particles. MA/GA ratios were <0.06 throughout

the experiment. Similar results were observed for blank experiments with polydisperse GA particles.

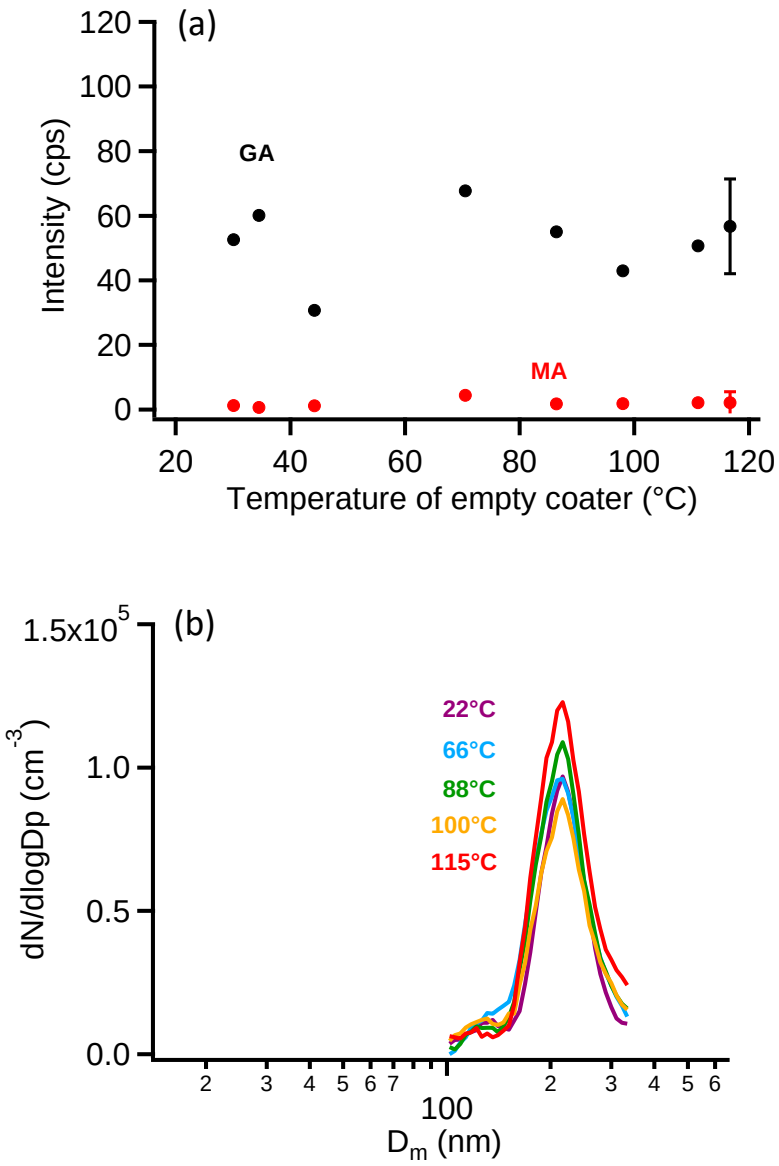

Figure S10. Blank experiment in which monodisperse GA particles (size-selected at 250 nm by DMA-1) were analyzed by EASI-MS while the coating reservoir was empty. (a) Signal intensities from orthogonal mode EASI-MS spectra of 220 nm GA particles (black) and MA (red) as a function of empty coater temperature. MRM intensities were averaged over approximately one minute. Error bars represent 1s uncertainties in replicate measurements. (b) Size distributions of monodisperse GA particles measured by SMPS as a function of temperature of the empty coating reservoir.

6. Malonic acid coating on 62 nm monodisperse glutaric acid particles.

Orthogonal EASI-MS measurements were carried out on GA particles size-selected at 100 nm with DMA-1 and measured by SMPS. Figure S11a shows several distributions in which the mode diameter increases with MA coating reservoir temperature. The peak appearing at <20 nm may be due to 62 nm particles that have accumulated +2 charges after size selection, but it is unclear what causes these smaller particles. This smaller diameter peak disappears as the particle coating accumulates. Mode diameters (Fig. S11a inset) indicate coating thicknesses become detectable at a coating reservoir temperature of ~80°C and reach 22 nm at 105°C. MRM particle signals are shown in Figure S11b to have a similar trend as the coated 220 nm monodisperse GA particles. MA/GA ratios are shown in Figure S11c in comparison to the bulk particle measurement for MA-coated 62 nm GA particles. Higher coating reservoir temperatures were reached but are not used in the analysis because the particle number concentration significantly increased, which indicated that MA self-nucleation may have been occurring.

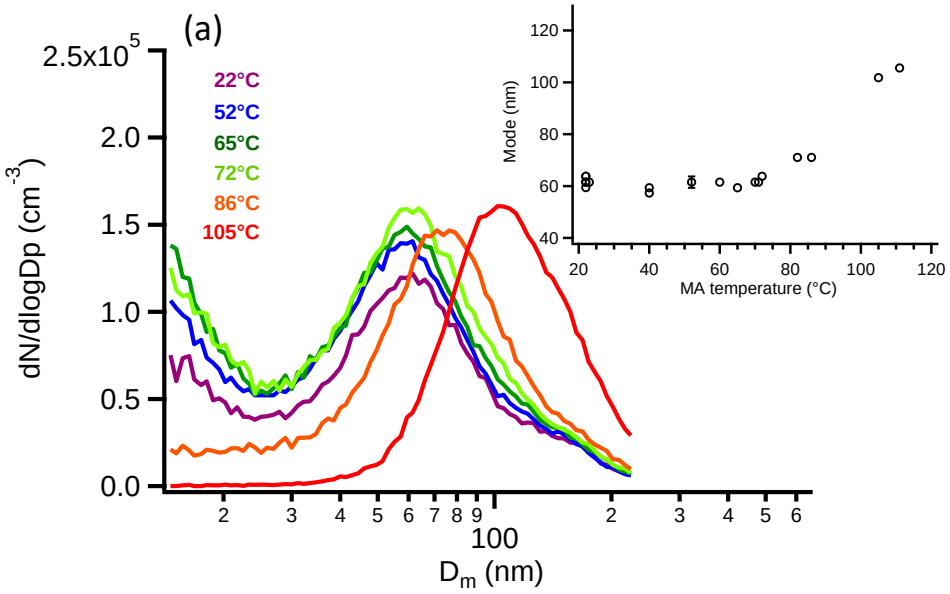
(a)
2.5x10^5
2.0
1.5
1.0
0.5
0.0
dN/dlogDp (cm^-3)
22°C
52°C
65°C
72°C
86°C
105°C
2 3 4 5 6 7 8 9 100 2 3 4 5 6
D_m (nm)
Mode (nm)
120
100
80
60
40
20 40 60 80 100 120
MA temperature (°C)

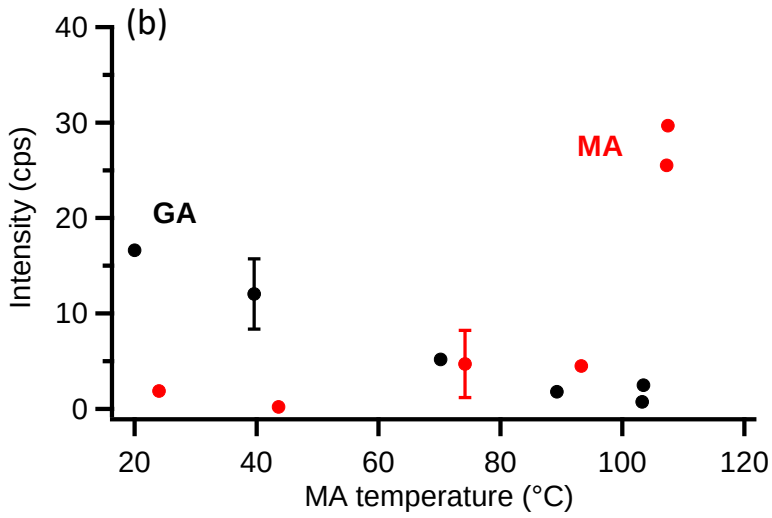
(b)
40
30
20
10
0
Intensity (cps)
GA
MA
20 40 60 80 100 120
MA temperature (°C)

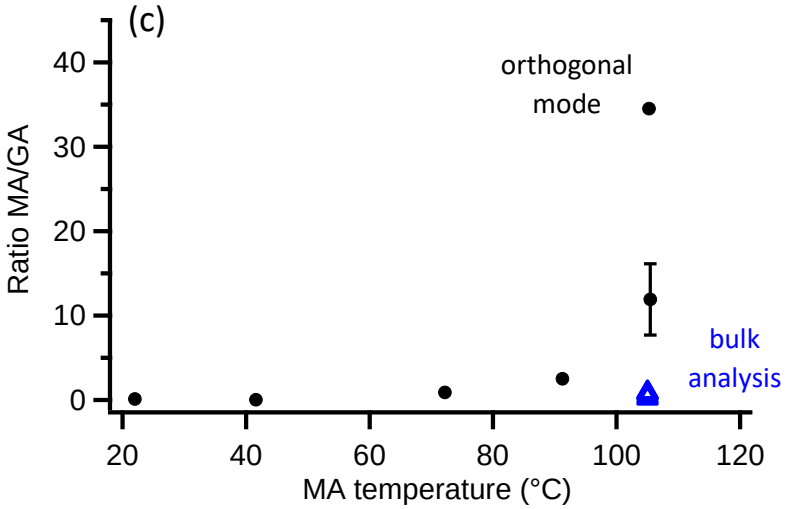
(c)
40
30
20
10
0
Ratio MA/GA
orthogonal
mode
bulk
analysis
20 40 60 80 100 120
MA temperature (°C)

Figure S11. Measurements from orthogonal EASI-MS experiments on monodisperse glutaric acid (GA) particles coated with malonic acid (MA). (a) Size distributions measured by SMPS for 100 nm size-selected GA particles (measured modes at 62 nm; see text) as a function of MA reservoir temperature and coating thickness. (b) Signal intensities from orthogonal mode EASI-MS spectra of 62 nm GA particles (black) coated with MA (red) as a function of MA reservoir temperature. MRM intensities were averaged over approximately one minute. (c) Black circles are the MA/GA ratios calculated from orthogonal EASI-MS data in (b); blue triangles are ratios from the bulk analysis of collected and extracted 62 nm GA particles (100 nm size-selected) coated with MA at 105°C. Error bars represent 1s uncertainties and are smaller than the markers for the bulk analysis.

7. Malonic acid coated on monodisperse pimelic acid particles.

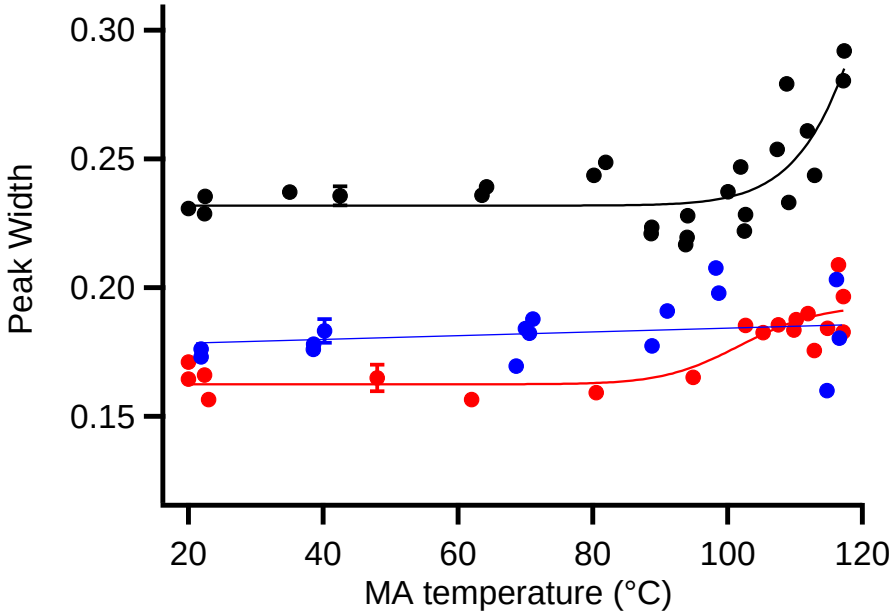

Figure S12. Peak widths of the size distributions of MA-coated PA (black), GA (blue), and SA (red) particles as a function of coating reservoir temperature/thickness. Peak width broadening is significant for the MA/PA system, indicating that these particles became more polydisperse as they were coated. Peak widths were obtained from log-normal fits of each size distribution as a function of MA coating temperature. Error bars represent 1s uncertainties.

References

1. Y. Dong, *Direct Analysis in Real Time Mass Spectrometry: Principles and Practices of DART-MS*, Wiley, 2017.
2. L. A. Doezema, T. Longin, W. Cody, V. Perraud, M. L. Dawson, M. J. Ezell, J. Greaves, K. R. Johnson and B. J. Finlayson-Pitts, *RSC Advances*, 2012, **2**, 2930-2938.
3. M. N. Clifford, V. Lopez, L. Poquet, G. Williamson and N. Kuhnert, *Rapid Commun. Mass Spectrom.*, 2007, **21**, 2014-2018.
4. M. Bilde, K. Barsanti, M. Booth, C. D. Cappa, N. M. Donahue, E. U. Emanuelsson, G. McFiggans, U. K. Krieger, C. Marcolli, D. Tropping, P. Ziemann, M. Barley, S. Clegg, B. Dennis-Smither, M. Hallquist, A. M. Hallquist, A. Khlystov, M. Kulmala, D. Mogensen, C. J. Percival, F. Pope, J. P. Reid, M. da Silva, T. Rosenoern, K. Salo, V. P. Soonsin, T. Yli-Juuti, N. L. Prisle, J. Pagels, J. Rarey, A. A. Zardini and I. Riipinen, *Chem. Rev.*, 2015, **115**, 4115-4156.
5. C. D. Cappa, E. R. Lovejoy and A. R. Ravishankara, *J. Phys. Chem. A*, 2007, **111**, 3099-3109.
6. C. Kidd, V. Perraud and B. J. Finlayson-Pitts, *Atmos. Environ.*, 2014, **82**, 56-59.
7. F. Tavakoli and J. S. Olfert, *Aerosol. Sci. Technol.*, 2013, **47**, 916-926.
8. T. J. Johnson, M. Irwin, J. P. R. Symonds, J. S. Olfert and A. M. Boies, *Aerosol. Sci. Technol.*, 2018, **52**, 655-665.
9. F. Tavakoli and J. S. Olfert, *J. Aerosol Sci.*, 2014, **75**, 35-42.
10. W. C. Hinds, *Aerosol Technology: Properties, Behavior, and Measurement of Airborne Particles*, John Wiley & Sons, Inc., 1999.
11. A. J. Prenni, P. J. DeMott and S. M. Kreidenweis, *Atmos. Environ.*, 2003, **37**, 4243-4251.
12. A. A. Zardini, S. Sjogren, C. Marcolli, U. K. Krieger, M. Gysel, E. Weingartner, U. Baltensperger and T. Peter, *Atmos. Chem. Phys.*, 2008, **8**, 5589-5601.
13. C. N. Cruz and S. N. Pandis, *Environ. Sci. Technol.*, 2000, **34**, 4313-4319.
14. A. Khlystov, *Aerosol. Sci. Technol.*, 2014, **48**, 604-619.
15. D. J. Rader, P. H. McMurry and S. Smith, *Aerosol. Sci. Technol.*, 1987, **6**, 247-260.